ACS Catalysis

Research Article

pubs.acs.org/acscatalysis

Ambient Oxidation of Benzene to Phenol by Photocatalysis on $Au/Ti_{0.98}V_{0.02}O_2$: Role of Holes

Perumal Devaraji,[†] Naveen K. Sathu,[†] and Chinnakonda S. Gopinath*[,†,‡,§]

[†]Catalysis Division, National Chemical Laboratory, Dr. Homi Bhabha Road, Pune 411 008, India

[‡]Network of Institutes for Solar Energy (NISE), NCL Campus, Dr. Homi Bhabha Road, Pune 411 008, India

[§]Centre of Excellence on Surface Science, National Chemical Laboratory, Dr. Homi Bhabha Road, Pune 411 008, India

Supporting Information

ABSTRACT: A potential photocatalyst with 2 atom % vanadium incorporated into the lattice of disordered mesoporous titania, $Ti_{0.98}V_{0.02}O_2$, (TV2) was synthesized. Au was deposited on TV2 (Au/TV2) through a photodeposition method. Structural, microscopy, and spectroscopy techniques support the incorporation of vanadium into the TiO_2 lattice, and Au was deposited on the surfaces of TV2. Photocatalytic oxidation of benzene was conducted at ambient temperature under UV and/or visible light to demonstrate the catalytic activity of the Au/TV2 catalyst. The TV2 lattice exhibits a quantum jump in benzene to phenol oxidation compared to that of TiO_2, highlighting the importance of V for oxidation. Introduction of Au onto TV2 further increases the benzene to phenol oxidation and phenol yield by a factor of 2 under UV light compared to those of bare TV2. No significant phenol production was observed in visible light with or without gold, indicating the role of gold is indirect toward charge separation and electron storage. Nano gold clusters on TV2 selectively store photoexcited electrons and in turn maximize holes utilization on TiO_2. The high photocatalytic activity of Au/TV2 is mainly attributed to the presence of Schottky junctions, disordered mesoporosity, and short diffusion lengths for charge carriers.

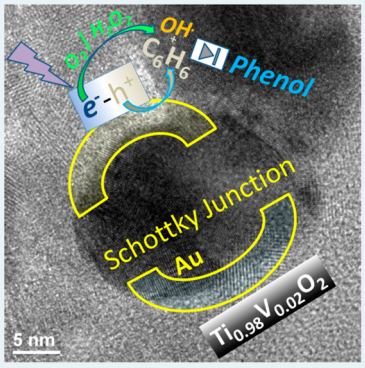

KEYWORDS: *titania, photocatalysis, phenol, vanadium, Schottky junction, nano gold*

1. INTRODUCTION

In green chemistry, photocatalysis plays an important role in solving some of the environmental issues. Of most of the semiconductor photocatalysts, TiO_2 plays a major role because of its extraordinary chemical stability by minimizing photocorrosion and its high oxidizing ability through holes produced upon light absorption.[1] The oxidation of benzene to phenol by photocatalysis is one of the important reactions attempted by many researchers, but without a significant breakthrough.[2−9] Direct oxidation of benzene through the cumene process[10] is a currently used method for the production of phenol that involves three steps; in this process, benzene and propylene are compressed to a pressure of 30 bar at 250 °C, in the presence of an acid catalyst, such as phosphoric acid. The disadvantage of this synthesis process is the formation of cumene hydroperoxide, which is an explosive, and acetone as a side product; this necessitates the discovery of a suitable new green method for phenol synthesis. Benzene to phenol oxidation on layered double hydroxides in one step has been reviewed recently.[11]

As early as 1981, Fujihira et al. demonstrated photocatalytic oxidation of toluene with TiO_2 in the presence of H_2O_2 and UV light from 500 W Xe lamp.[2] Palmisano et al. reported selective photocatalytic oxidation of 4-methoxy benzyl alcohol to the corresponding aldehyde in an aqueous suspension of TiO_2 catalyst under UV light.[3] Ide et al.[4] showed a 62% yield with a 96% phenol selectivity for photocatalytic benzene oxidation in visible light with layered titanate containing immobilized gold nanoparticles in the interlayer space. However, this result is possible only when the initial amount of benzene is a few hundred parts per million (x) but in the presence of large excess of a seed amount of phenol ($\geq 10x$). When there is no seed phenol added, there is no phenol production observed.[4a] Ide et al. also reported benzene oxidation over Au/TiO_2 with a 13% yield and a 89% phenol selectivity after 24 h under a CO_2 atmosphere (230 kPa) under 1 sun irradiation conditions.[4b] A high phenol yield (~60%) with highly dispersed Au on TiO_2 in visible light was demonstrated by Zheng et al.;[5] a high level of Au dispersion was possible due to prereduction of titania to blue titania (contains Ti^{3+}), either by UV photoreduction[5a] or by Zn^{2+} doping in titania,[5b] and helps to reduce gold ions in a uniform manner with Schottky junctions. Benzene oxidation was conducted in a manner similar to that described in ref 4a. Fe-doped g-carbon nitride coated on SBA-15 exhibits 11.9% benzene conversion with 20.7% phenol selectivity at 60 °C in visible light.[7] Selective photocatalytic oxidation of benzene to phenol (38% benzene conversion and 97% phenol selectivity) was demonstrated on an $FeCl_3$/mpg-C_3N_4 hybrid with $\lambda \geq 420$ nm at 60 °C; the same catalyst shows only 4% benzene

Received: January 22, 2014
Revised: July 3, 2014
Published: July 15, 2014

   dx.doi.org/10.1021/cs500724z | ACS Catal. 2014, 4, 2844−2853

conversion.[8] The survey described above highlights the challenges involved in designing a new photocatalyst that gives a high benzene conversion and a high phenol selectivity at ambient temperature and pressure in the field of photocatalysis.

Monomeric or isolated V is known to be a good partial oxidation or oxidative dehydrogenation catalyst.[12] Because of the high partial oxidation nature associated with isolated V, it is worth exploring vanadium doped into the lattice of TiO_2 (V/TiO_2) under the photocatalytic conditions. V/TiO_2 is useful not only for benzene oxidation but also for many other oxidation reactions.[13−18] Earlier, Tanarungsun et al. showed the photocatalytic activity of vanadium-impregnated TiO_2 for benzene oxidation under a UV light source with a 0.19% yield and a 90% selectivity.[6] It is important to keep the V in an isolated or monomeric state for the desired partial and selective oxidation. It is also essential to prepare the V/TiO_2 system with mesoporosity for better activity. Although the ordered mesoporous material shows a large surface area, the reactant and product molecules have to diffuse a long distance to and from the active sites that are present in the mesopores. This is due to the availability of more active sites on the surface of porous channels. Hence, the presence of a short diffusion length associated with disordered mesopores is likely to be helpful in minimizing the diffusion problem.[19−21] This is expected to improve the catalytic activity and selectivity of the desired product.

In this study, we have synthesized 2 atom % V doped in anatase TiO_2 (TV2, $Ti_{0.98}V_{0.02}O_2$) by the solution combustion method (SCM)[12,22] and analyzed its photocatalytic activity for the oxidation of benzene to phenol in a biphasic system under UV−visible light under ambient conditions. The photodeposition method was used to deposit Au on TV2 (Au/TV2), producing 18% benzene conversion with phenol selectivity and yields of 88.1 and 15.9 mol %, respectively, after UV irradiation with Au/TV2 for 18 h. This study is a part of various efforts from our laboratories to synthesize rationally designed photocatalytic materials.[23]

2. EXPERIMENTAL SECTION

2.1. Preparation of the Catalysts. All the chemicals employed in this study were of analytical grade and used as such. Titanium isopropoxide as a Ti precursor, ammonium metavanadate as a V precursor, and urea as a fuel were used. The procedure followed for the synthesis of TV2 by SCM was previously reported by our group.[12] The synthesis of V-doped TiO_2 was conducted with a 1:1 molar ratio of urea to metal ions (Ti and V). The required amount of reactants was taken in a 250 mL beaker, and the aqueous solution was stirred for 1 h, followed by introduction of the solution described above into a muffle furnace preheated at 400 °C. Evaporation of water starts at the beginning followed by smoldering-type combustion that results in a powder material. Similarly, TiO_2 was synthesized without adding any V precursor.

Gold deposition was conducted by the photodeposition method using $HAuCl_4$ as the gold precursor. In a 250 mL quartz round-bottom flask, 30 mL of required $HAuCl_4$ was taken in 120 mL of MeOH with 500 mg of catalyst. The solution described above was bubbled with Ar at a rate of 50 mL/min for 1 h to remove any dissolved oxygen and generate an inert atmosphere. Irradiation with a 400 W UV lamp was conducted for 1 h (λ = 200−400 nm). After photodeposition, the powder sample was separated by centrifugation, and finally, the Au-deposited powder sample was dried at 40 °C for 12 h. Two samples were prepared by changing the molar concentration of $HAuCl_4$. The sample with a concentration of 0.0005 M was named 1Au/TV2, and the sample with a molar concentration of 0.0015 M was named 3Au/TV2. ICP analysis shows the Au content to be 0.95 and 2.92 wt %, and they are denoted as 1Au and 3Au, respectively, as shown above.

2.2. Characterization. To explore the structural properties of as-synthesized materials, different characterization techniques have been used, such as high-resolution transmission electron microscopy (HRTEM), scanning electron microscopy (SEM), powder X-ray diffraction (PXRD), N_2 adsorption−desorption isotherms, photoluminescence (PL), energy dispersive X-ray analysis (EDX), and X-ray photoelectron spectroscopy (XPS). PXRD data were collected from a PAN analytical X'pert Pro dual goniometer X-ray diffractometer, using Cu Kα (1.5418 Å) radiation with a Ni filter, and the data were collected using a flat holder in Bragg−Brentano geometry (0.2°). The SEM system equipped with an EDX attachment (FEI, model Quanta 200 3D) was used for morphological and chemical composition. The surface area and pore size distribution of the materials were analyzed on a Quadrasorb SI instrument; the measurement was conducted after the materials had been degassed at 200 °C. HRTEM of the materials was conducted on a FEI TECNAI 3010 electron microscope operating at 300 kV (Cs = 0.6 mm; 1.6 Å resolution). Raman spectra of the samples were analyzed with a Horiba JY LabRAM HR 800 Raman spectrometer coupled with a microscope in reflectance mode with a 633 nm excitation laser source and a spectral resolution of 0.3 cm^{-1}. XPS measurements have been taken with a custom-built ambient-pressure XPS system from Prevac and equipped with a VG Scienta SAX 100 emission controller monochromator using an Al Kα anode (1486.6 eV) in transmission lens mode.[24] The photoelectrons are energy analyzed using VG Scienta's R3000 differentially pumped analyzer. PL measurements were performed using a Horiba Jobin Yuon Fluorolog 3 spectrophotometer equipped with a 450 W xenon lamp with a tunable excitation wavelength. All PL measurements were taken with 325 nm excitation pulses. Diffuse reflectance UV−vis measurements were taken on a Shimadzu spectrophotometer (model UV-2550) with spectral-grade $BaSO_4$ as reference material.

2.3. Photocatalytic Activity and Photocurrent Measurements. Photocatalytic oxidation reactions were conducted in a quartz RB flask for different periods of time with a 400 W mercury lamp (λ = 200−400 nm) using a flow-type double-jacketed quartz reactor.[23] In a typical experiment, 30 mg of the catalyst was dispersed in a quartz RB flask, containing an initial reactant mixture of 2 mL of CH_3CN, 1 mL of benzene, and 2 mL of 25% H_2O_2. Unless mentioned otherwise, dissolved oxygen in the solution described above was not removed. Few irradiation experiments were conducted with a WG.305 filter to block the radiation between 200 and 309 nm. The temperature of the double-jacketed reactor and quartz RB was maintained at 25 °C by allowing water circulation. Before any irradiation, the reaction mixture was stirred for 30 min in the dark and irradiation was conducted for different lengths of time between 6 and 24 h. After irradiation, organic and aqueous layers were separated with a separating funnel. Oxidized products of benzene were analyzed with an Agilent 6890 gas chromatograph (GC) equipped with a flame ionization detector (FID) and an HP-5.5% phenyl methyl siloxane capillary column. The presence of phenol was confirmed by analyzing both organic and aqueous layers. It is to be noted that the presence of any

dx.doi.org/10.1021/cs500724z | ACS Catal. 2014, 4, 2844−2853

other liquid products in the chromatogram was included in the quantitative estimation.

Chronoamperometry measurments were recorded at 0 V using a Gamry potentiostat (model 3000 potentiostat/galvanostat/ZRA) in a conventional three-electrode test cell with Ag/AgCl as the reference electrode and a platinum foil as the counter electrodes with an Oriel Instruments 300 W xenon arc lamp equipped with an A.M 1.5 filter.[23] The immediate response for shutter oscillation highlights the photofunctional behavior of the material. As long as the material is irradiated, the current remains constant, demonstrating production of the current is exclusively due to the photoresponse.

3. RESULTS AND DISCUSSION

3.1. Structural and Textural Properties Determined by X-ray Diffraction Studies. PXRD studies have been conducted to explore the structural aspects of prepared catalysts. Figure 1 shows the PXRD pattern of all catalysts

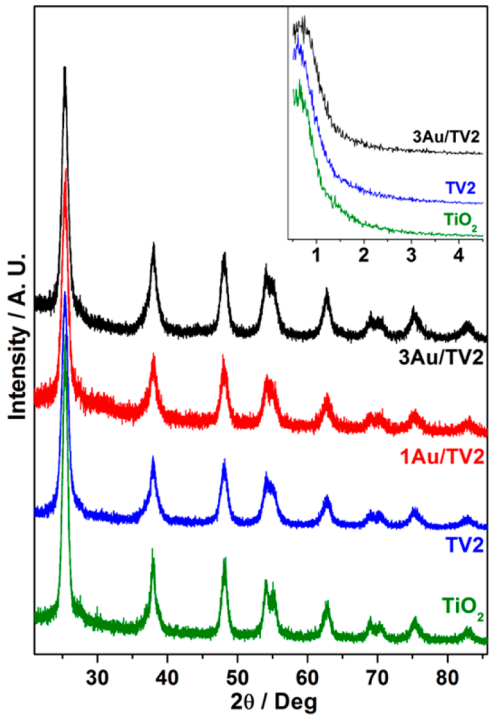

Figure 1. XRD pattern of different materials, namely, TiO_2, TV2, 1Au/TV2, and 3Au/TV2. The inset shows the low-angle XRD pattern, indicating its disordered mesoporous nature.

prepared by SCM. The PXRD pattern of all materials was found to match that of the anatase phase (JCPDS Card No. 21-1272). No peaks corresponding to oxides of vanadium are observed, which indicates that TiO_2 and TV2 retain the anatase phase with no V_2O_5 phase. No V_2O_5 formation in TV2 indicates the potential of the SCM method to introduce V into the TiO_2 lattice. The broad nature of the peaks confirms the presence of nanocrystalline particles. No peaks were observed for metallic Au in 1Au/TV2 or 3Au/TV2, which indicates a high level of dispersion of Au on TV2. The respective average crystallite size, calculated from the peak width with the Scherrer equation, is observed to be between 8 and 12 nm. The inset of Figure 1 shows the low-angle XRD pattern. A single diffraction peak observed around 0.8° demonstrates the mesoporous nature of the $Ti_{1-x}V_xO_2$ materials. Unlike ordered mesoporous materials, such as SBA-15 and MCM-48, all TV2 and titania materials exhibit only one peak around 0.8° without any extra peaks.[25] This highlights the presence of disordered mesoporosity[12,19−21] for all TV2 materials.

3.1.1. Surface Area Analysis. N_2 adsorption−desorption studies have been conducted to investigate the textural properties of mesoporous TiO_2, TV2, 1Au/TV2, and 3Au/TV2 materials. Figure 2a shows the results of N_2 adsorption−desorption isotherm studies conducted at 77 K and analyzed by the BET method for surface area, and Figure 2b the Barret−Joyner−Halenda (BJH) pore size distribution of TiO_2 and all TV2 materials. The surface area and porosity have been calculated for all of the materials, and the results are listed in Table 1. All TV2 materials show a type IV adsorption−desorption isotherm with an H2 hysteresis loop that clearly indicates the presence of mesopores.[21,23] An average pore size distribution in the range of 4.5 ± 2 nm and an overall pore volume of 0.26 ± 0.02 cm^3/g were observed. TV2 exhibits a surface area (166 $m^2\ g^{-1}$) larger than that of TiO_2 (117 $m^2\ g^{-1}$). This indicates that when gold was introduced onto the surface of TV2, the surface area decreased marginally compared to that of TV2. Because of the high level of dispersion of gold nanoparticles on TV2, the surface area of 3Au/TV2 (151 $m^2\ g^{-1}$) is similar to that of 1Au/TV2 (156 $m^2\ g^{-1}$). The pore size distribution profile indicates the presence of mesopores in all of the catalysts. A significant shift in pore size toward a lower value is evident for 3Au/TV2 (Figure 2b), highlighting the introduction of gold nanoclusters into pores, too.

3.1.2. HRTEM and SEM. The morphology and textural properties of TV2 and Au/TV2 materials were analyzed by HRTEM and SEM, and representative images are shown in Figure 3. Generally, TV2 and 1Au/TV2 (and TiO_2, not shown) exhibit spherical particles and disordered mesoporous structures (Figure 3a−c). TV2 and Au/TV2 materials show textural characteristics similar to those of TiO_2.[21] Disordered mesoporosity arises from the intergrowth of fundamental particles, and the same leads to aggregates with significant extra framework void space.[20,26,27] The nanocrystalline nature and anatase phase of the materials were confirmed by the selected-area electron diffraction (SAED) pattern. HRTEM shows a particle size of ∼14 nm with a *d* spacing of 0.35 nm, which corresponds to the (101) plane of the TiO_2. These results are supported well by XRD as well as N_2 adsorption isotherm results. The disordered mesoporous structure has additional advantages like low diffusional barriers, because the depth of mesopores is minimal, a few nanometers, unlike values of several hundred nanometers in conventional ordered mesoporous materials, like SBA-15.[25] These types of mesopores are known as pseudo three-dimensional (*p*3D) mesopores.[21] This disordered *p*3D mesoporous framework provides an easy route for the diffusion of reactants due to lower diffusion barriers as well as short diffusion lengths due to the small meso channel depth. Figure 3b demonstrates the particles are electrically interconnected together, which helps for the fast mobility of charge carriers to the surface of the catalyst where the reaction could occur.

The presence of gold is clearly visible by HRTEM (Figure 3b,c). The measured *d* spacing is 0.24 nm, which corresponds to the (111) plane of metallic Au. The size of the gold particle is approximately 7−8 nm; however, smaller particles were also observed. The binding energy for typical metallic gold was observed in XPS (*vide infra*) underscores the nature of gold particles to be metallic on Au/TV2. Very importantly, the Au−

dx.doi.org/10.1021/cs500724z | ACS Catal. 2014, 4, 2844−2853

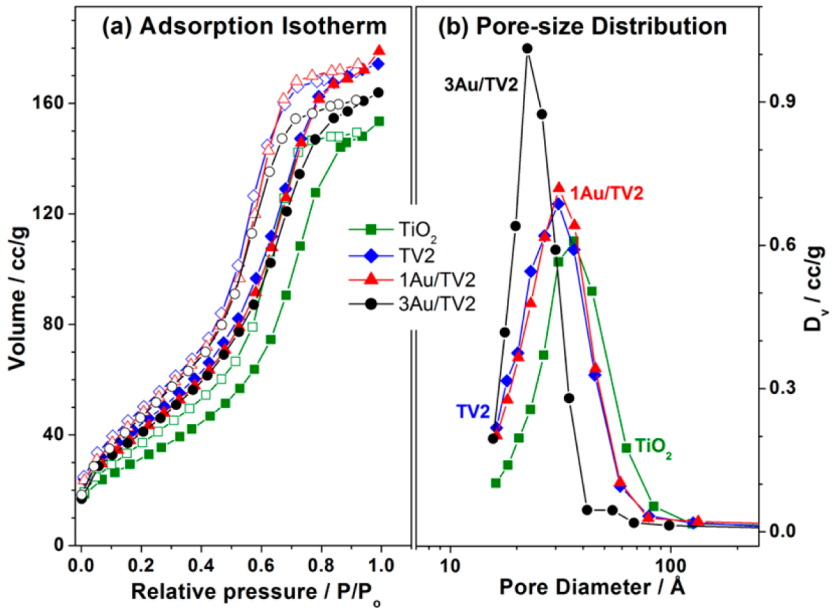

Figure 2. (a) N_2 adsorption−desorption isotherm and (b) pore size distribution pattern of TiO_2, TV2, and Au/TV2 materials.

Table 1. Physicochemical Properties of TiO_2, TV2, and Au/TV2 Catalysts

catalyst	BET surface area (m^2/g)	pore size (nm)	pore volume (cm^3/g)
TiO_2	117	6.2	0.24
TV2	166	4.6	0.27
1Au/TV2	156	6.2	0.28
3Au/TV2	151	4.4	0.25

TiO_2 metal−semiconductor (Schottky) junction was observed easily with Au/TV2; (111) facets of nano gold are in direct contact with (101) facets of titania shown in panels d and e of Figure 3. Indeed, this is a criticial feature of Au/TV2 catalysts that is essential for the separation of the charge carriers and hence enhances the diffusion of charge carriers toward the surface of the catalysts from the bulk. Both V and Au could act as electron-trapping centers, and hence, the extent of hole utilization increases significantly. This also leads to a decrease in the level of charge recombination. In fact, this observation is in good agreement with PL results, which show an increase in the level of electron transfer and hence an increase in the number of emission features compared to that of TV2.

3.2. Absorption and Emission Properties Determined by UV−Visible Absorption Studies. UV−visible absorption was measured to study the optical properties and examine the deposition and doping effect of Au and V, respectively, on TiO_2. Figure 4 depicts the UV−vis absorption spectra, and the inset shows the color associated with TiO_2, TV2, and Au/TV2 materials. TiO_2 shows absorption up to 380 nm in the UV region with a 3.2 eV band gap, which is typical for titania. V doping increases the level of visible light absorption up to 560 nm in TV2 catalysts. The visible light absorption in TV2 is attributed to low-energy charge transfer bands originating from charge transfer between O 2p and V 3d. This band position is influenced by the coordination and oxidation state of V. The V^{5+} state leads to absorption up to 550 nm, whereas V^{4+} leads to a d−d transition band between 550 and 800 nm;[12c,28] the latter is absent in our study, suggesting the oxidation state to be V^{5+} in TV2. This is also in agreement with XPS studies. The

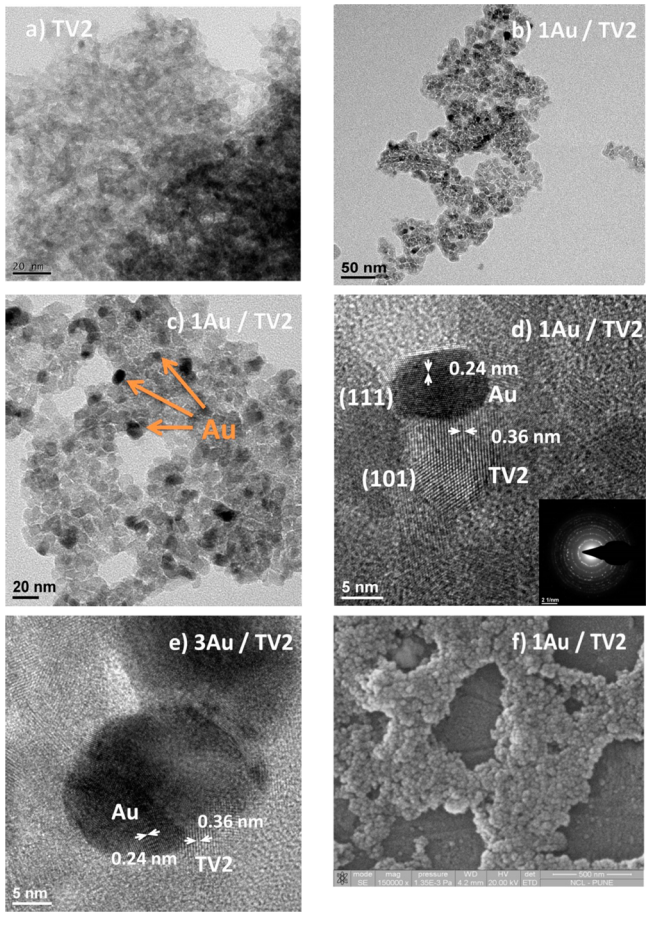

Figure 3. TEM images of (a) TV2 and (b and c) Au/TV2, HRTEM images of (d) 1Au/TV2 and (e) 3Au/TV2, and (f) SEM image of 1Au/TV2. Abundantly available Schottky junctions between (111) facets of nano Au cluster and (101) facets of titania particles are shown in panels d and e. The SAED pattern given in panel d shows (101) is the major facet of TiO_2 exposed on the surfaces.

dx.doi.org/10.1021/cs500724z | ACS Catal. 2014, 4, 2844−2853

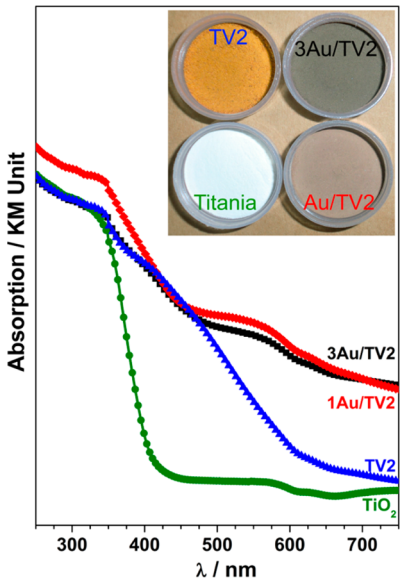

Figure 4. UV–vis spectra of TiO_2, TV2, 1Au/TV2, and 3Au/TV2 materials.

absorption intensity in the visible region, between 500 and 600 nm, is significantly enhanced after the deposition of Au on TV2, and this is attributed to the surface plasmon resonance (SPR) absorption by nano gold clusters.[25] Strong interaction between Au and TV2 leads to the enhancement of visible light absorption, and Schottky junction helps for the separation of charge carriers. However, nano gold does not absorb significant UV light to demonstrate SPR, because of the poor absorption coefficient.

3.2.1. Photoluminescence Studies. Figure 5 shows the PL emission spectra of TV2 materials measured with an excitation

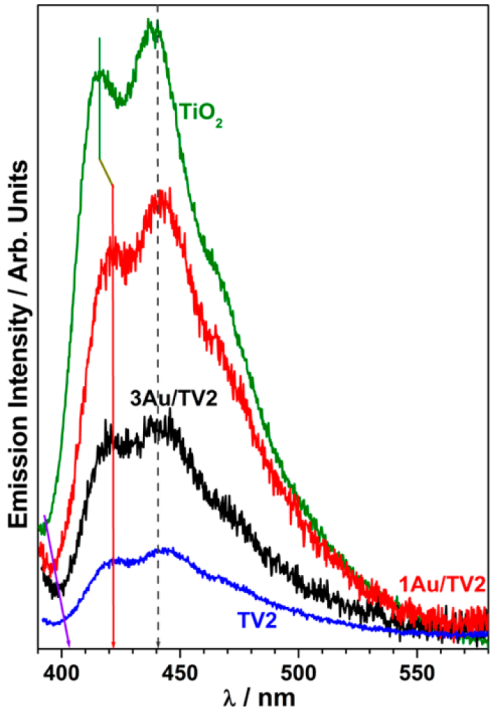

Figure 5. Photoluminescence (PL) spectra of TiO_2, TV2, 1Au/TV2, and 3Au/TV2 materials.

wavelength 325 nm. TiO_2, TV2, and Au/TV2 composites show emission features around 415, 441, and 470 nm, respectively. The emission peak due to the band gap transition appears at 380 nm for all materials (not shown). A high-intensity emission feature at 441 nm originates from the charge transfer transition from Ti^{3+} to the oxygen anion in a $[TiO_6]^{8-}$ complex present on the material along (101) planes.[29] The emission band at 415 nm is attributed to the free exciton emission of TiO_2. After the sample had been doped with V, a significant red shift in the first emission band to 422 nm was observed, while no shift was observed with the latter two emission features.

This observation underscores the introduction of new acceptor states below the CB, due to the reduction of V^{5+}, which is supported by UV–vis absorption and XPS studies. Further, the onset of emission of the first band also shifts from titania to TV2 by the same extent. All three emission features show the lowest intensity for TV2 and the highest for undoped TiO_2, indicating a significant electron trapping by doped V in TV2. This process makes the holes available for oxidation on the titania surface and leads to charge separation. Nonetheless, upon deposition of Au on TV2, the intensity of all emission features was observed to be higher than that of TV2;[25b] 1Au/TV2 exhibits an emission intensity higher than that of 3Au/TV2. It is to be underscored here that the anatase (101) facet is the most abundant plane (Figure 3) and corrugated with alternating rows of five-coordinated Ti (Ti^{3+}) and bridging oxygen at the edges of corrugation.[30] This fact suggests the reduction of Ti due to V doping. The five-coordinated surface Ti^{3+} makes (101) an ideal facet for interaction with deposited nano Au clusters due to a high level of surface unsaturation. In fact, the interaction described above also reiterates the presence of Schottky junctions in Au/TV2 nanocomposites, which helps in electron–hole separation at the interface of Au and TiO_2.[5,24] The presence of Schottky junctions was directly supported by HRTEM measurements, which supports the conclusion described above. Indeed, this is an important observation that indicates the surface electronic interaction between nano Au clusters and TV2. Further, as nano metal clusters are a good electron sink, they separate and store electrons and make the holes available predominantly for oxidation. In essence, electron trapping by V^{5+} on TV2 and electron storage by gold clusters on Au/TV2 through Schottky junctions work simultaneously and lead to an overall increase in hole availability and/or level of utilization for the oxidation reaction. When additional Au is loaded (3Au/TV2), the intensity of all emission features decreases. Nonetheless, Au/TV2 exhibits emission features with an intensity higher than that of TV2, which underscores the transfer of an electron from nano Au to the CB of titania. The decrease in the intensity of 3Au/TV2 emission features is due to an increase in the size of the gold cluster (Figure 3e) and hence a weakened interaction with the surface. On the basis of PL spectra, it can be inferred that materials prepared by the SCM method show a substantial decrease in their level of charge recombination due to selective electron trapping by V and nano gold clusters, which enhances the utilization of holes for oxidation.

3.2.2. Raman Spectroscopy. Figure 6 shows the Raman spectra of all catalysts compared with that of V_2O_5 as a reference. All the catalysts show Raman active fundamental modes[12,31] for the anatase phase of titania. It is observed that the intensity of all the Raman active modes decreases, and broadening occurs after V doping. This decrease in the peak intensity for TV2 and Au/TV2 reveals symmetry breaking of

dx.doi.org/10.1021/cs500724z | ACS Catal. 2014, 4, 2844–2853

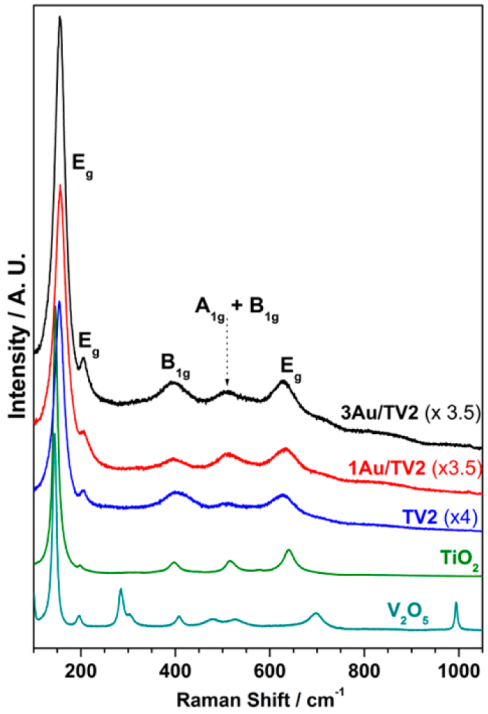

Figure 6. Raman spectra of the V_2O_5, TiO_2, TV2, 1Au/TV2, and 3Au/TV2 samples.

TiO_2 due to incorporation of "V" into the crystallographic lattice position of TiO_2.[12a,31] Hence, Raman results support the lattice doping of V in TiO_2. Also, peak broadening confirms the presence of a nanocrystalline particle, and these results are consistent with XRD results. In the case of TV2 and Au/TV2, a small shift in the peak at 145 cm^{-1} is observed, and it confirms doping of "V" into the TiO_2 lattice. No characteristic peaks are observed for V_2O_5, which indicates the absence of any V_2O_5 phase with the TV2 or Au/TV2 catalyst.[32]

3.3. X-ray Photoelectron Spectroscopy. XPS studies were conducted to analyze the electronic states of TV2 catalysts. Figure 7 shows XPS spectra of Ti 2p, V $2p_{3/2}$, and Au 4f core levels of TV2 and Au/TV2 materials. The Ti $2p_{3/2}$ core level of TiO_2, TV2, and Au/TV2 appears at a binding energy (BE) of 459.1 ± 0.1 eV, and it confirms the presence of Ti^{4+} in all of the materials.[33] V doping in the titania lattice shows a V $2p_{3/2}$ peak at a BE of 517.3 eV for TV2 as well as Au/TV_2, indicating the oxidation state of V is predominantly +5 (Figure 7a, inset). It should be noted that the surface atom percent of V increases from 0.4% on TV2 to 0.7% on 3Au/TV2; however, the bulk atom percent of V remains at 1.9%, measured from ICP analysis. The O 1s core level was observed at a BE of ~530 ± 0.2 eV for all materials (data not shown). Au 4f (Figure 7b) core level spectra of 1Au/TV2 show at BE of Au $4f_{7/2}$ at 83.8 eV; it corresponds well to the BE of metallic gold at 84.0 eV.[34] These results suggests that gold and V are present in the metallic state (Au^0) and V^{5+}, respectively.[25] The electronic interaction described in the preceding sections does not induce an observable shift in the BE in XPS.

3.4. Photocatalytic Benzene Oxidation. Panels a and b of Figure 8 show the photocatalytic activity measured with a TV2 catalyst at different time intervals for benzene to phenol oxidation under UV irradiation. Figure 8c shows the phenol yield observed with TV2 and Au/TV2 catalysts after irradiation for 18 h. TV2 shows a 3% benzene conversion with a 100% selectivity after irradiation for 6 h. The level of benzene conversion increased linearly from 3 to 13% with an increasing irradiation time from 6 to 24 h, respectively; however, a significant decrease in phenol selectivity [from 100 to 85% (Table 2)] was also observed. The decrease in phenol selectivity is mainly due to further oxidation of phenol to other side products, such as hydroquinone. Also, a qualitative

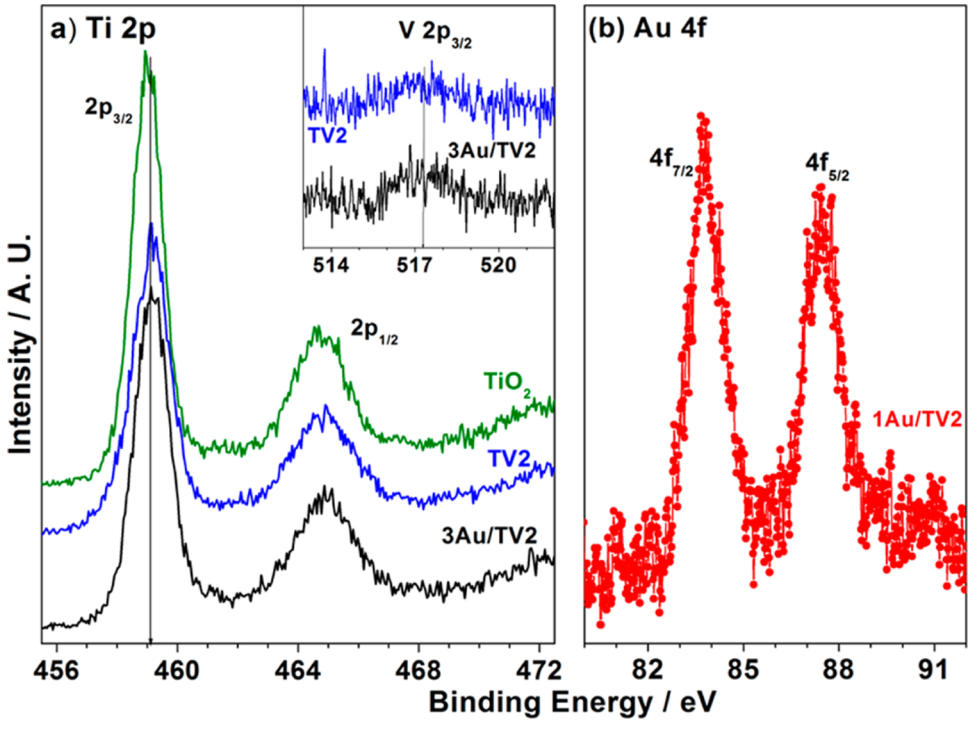

Figure 7. XPS spectra recorded for (a) Ti 2p and V 2p in the inset and (b) Au 4f core levels of TiO_2, TV2, and Au/TV2 catalysts.

dx.doi.org/10.1021/cs500724z | ACS Catal. 2014, 4, 2844−2853

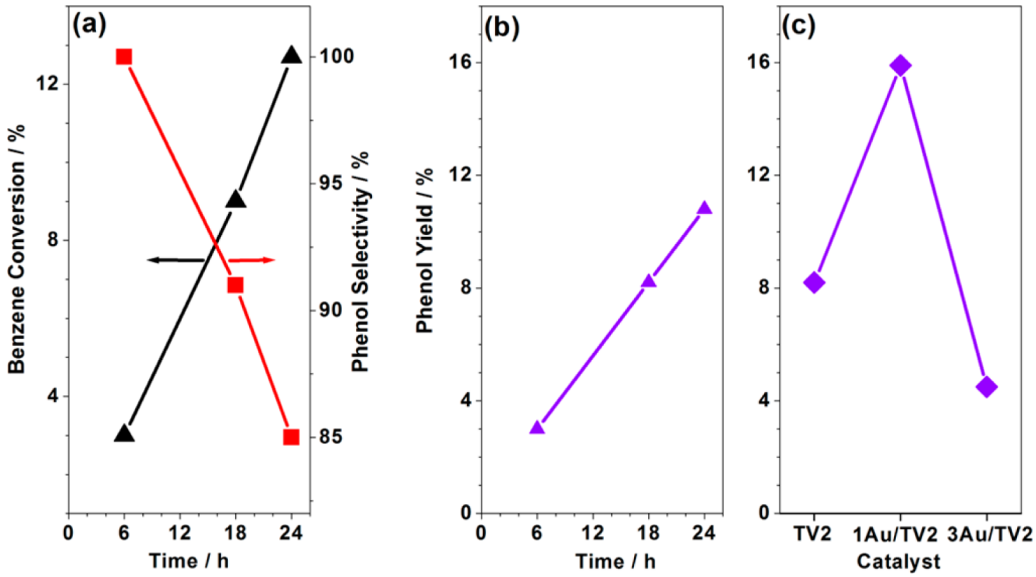

Figure 8. UV irradiation time dependence of photocatalytic benzene oxidation results for (a) benzene conversion and phenol selectivity with TV2 and (b) phenol yield with TV2. (c) Phenol yield observed with TV2, 1Au/TV2, and 3Au/TV2 after UV irradiation for 18 h.

Table 2. Photocatalytic Benzene Oxidation Measured under Different Conditions

			phenol	
catalyst and irradiation conditions[a]	*t* (h)	benzene conversion (%)	yield (%)	selectivity (%)
TV2 with UV	6	3.0	3.0	100
TV2 with UV	18	9.0	8.2	91
TV2 with UV	24	12.7	10.8	85
1Au/TV2 with UV	18	18.0	15.9	88
3Au/TV2 with UV	18	5.0	4.5	90
TiO_2 with UV	24	0.3	0.3	100
TV2 with visible	24	0.4	0.4	100
1Au/TV2 without visible	24	2.0	2.0	100
no catalyst with UV	18	5.5	3.3	61
1Au/TV2 with UV[b]	18	3.0	2.9	97
no catalyst with UV (λ > 300 nm)	18	1.2	0.6	50

[a]Unless mentioned otherwise, the reaction was conducted with H_2O_2, H_2O, and CH_3CN. [b]Dissolved oxygen was removed by argon bubbling for 30 min.

analysis of gaseous products shows hydrogen and CO_2, indicating the re-formation of organic compounds via secondary reactions. This diverts some amount of charge carrier to the secondary reactions described above and hence affects the selectivity and yield of the primary product (phenol). However, we believe it occurs mainly to maintain the charge neutrality of the system, which prevents the accumulation of electrons in gold clusters and TV2. Table 2 displays a set of benzene oxidation results with different catalysts using UV and visible light radiation. 1Au/TV2 (TV2) shows 18% (9%) benzene conversion and 16% (8.2%) phenol yield after UV irradiation for 18 h. A simple doubling of the catalytic activity after gold deposition highlights the importance of Au in selectively separating and storing electrons from excitons. The catalyst with high concentration of Au (3Au/TV2) gives a low benzene conversion (5%) and a low phenol yield (4.5%); these results are reproduced with catalysts prepared in the same and different batches. The low activity observed with 3Au/TV2 is attributed to two reasons, namely, the formation of large gold clusters on TV2 due to a large amount of gold deposition (Figure 3e). Further, a large amount of gold also hinders the absorption of light, and hence, the extent of light utilization becomes relatively low. This reiterates the necessity of an optimal amount of gold.

Many control experiments were also conducted, such as benzene oxidation without a catalyst. In the dark or without irradiation, there is no reaction whatsoever. Irradiation for 18 h without a catalyst induces photochemical oxidation of benzene, and the results are surprisingly comparable to those for 3Au/TV2. However, a large amount of side products is observed in the case without a catalyst, indicating the possibility of an exclusive free radical mechanism due to photochemical conversion and homogeneous cleavage of hydrogen peroxide decomposition. The spectral output of a UV lamp source shows the UV C radiation between 240 and 300 nm (see Figure S1 of the Supporting Information). When the incident photons are filtered for λ < 309 nm, very little photochemical conversion was observed; however, no significant change in conversion or selectivity was observed with TV2 and Au/TV2 catalysts. This indicates the photochemical conversion was high with high-energy UVC radiation, even without a catalyst. In the presence of visible light on 1Au/TV2, the activity is also poor, with a 2% phenol yield. Indeed, this highlights that gold does not have any role as a catalyst. Although Au nanoclusters absorb visible light due to SPR, only electrons can be transferred to the CB of titania, leaving the holes in gold clusters. This aspect is verified by photoelectrochemical measurements. Chronoamperometry measurements were taken on TV2 and 1Au/TV2 under AM1.5 irradiation (1 sun condition), and the results are shown in Figure 9. Compared to TV2, 1Au/TV2 generates an at least 5-fold higher current under irradiation conditions, demonstrating the effective absorption of visible light by gold in Au/TV2. When the light was cut off by closing the shutter, no current was produced, demonstrating the photofunctional behavior of Au/TV2 in visible light. A small amount of current produced by TV2 is likely due to absorption of a small amount of UV by titania. Because TV2 is the active part of the catalyst and no holes are available on the same under visible light conditions,

dx.doi.org/10.1021/cs500724z | ACS Catal. 2014, 4, 2844−2853

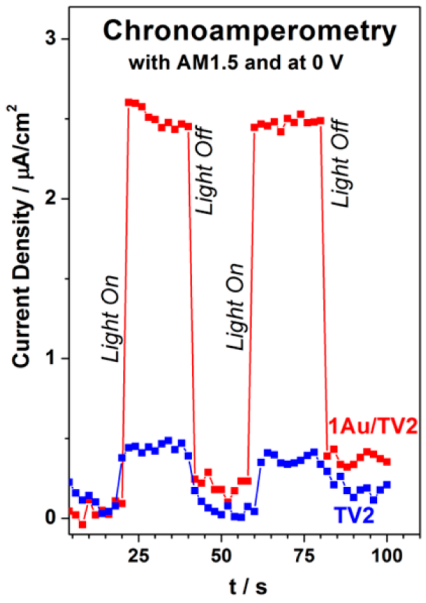

Figure 9. Chronoamperometry measurements taken at zero voltage for TV2 and Au/TV2 with simulated sunlight with an AM1.5 filter.

the activity is poor. The highest activity observed in UV light underscores the necessity of energetic holes on the titania surface, which can be met only by UV radiation. The low activity in visible light with Au/TV2 confirms the importance of the role of holes on TV2 surfaces. TiO_2 without V doping also shows minor activity, underscoring the role of V for charge separation.

Another important aspect of the reaction is the presence of dissolved oxygen in the reactant solution. Argon was bubbled through the reactant solution to remove dissolved oxygen, and photocatalytic conversion was measured with 1Au/TV2 (Table 2). Surprisingly, the benzene conversion and phenol yield decreased, while high selectivity was maintained. This result underscores the role of oxygen[9] in producing hydroxyl radicals, which is a well-known pathway.[35] Total oxidation of the aqueous solution of benzene to CO_2 through phenol with molecular oxygen was addressed by Bui et al.,[9] and this study demonstrates the necessity of molecular oxygen and the oxygen from water for oxidation. Nonetheless, without a peroxide source, there is no reaction observed with dissolved oxygen alone. Our experiments demonstrate that the co-presence of molecular oxygen with H_2O_2 is necessary for high benzene conversion as well as phenol yield. This indicates that both act synergistically to increase the activity. Indeed, the role of dissolved oxygen makes this reaction a total green chemistry reaction.

3.5. Proposed Mechanism. On the basis of the photocatalysis experiments conducted with different catalysts and conditions, material characterization results through different spectroscopy and structural techniques, chronoamperometry results under visible light, and available experimental results such as oxidation potential of benzene, from literature, a possible mechanism of benzene oxidation is proposed in Figure 10. In the proposed mechanism, charge carriers are generated upon absorption of light by TiO_2. The generated holes in the VB of titania react with benzene molecule and generate benzene radical ions; electrons are consumed by peroxide (not shown) as well as by oxygen molecules to form hydroxyl radicals via superoxide formation (Figure 10).[35] The superoxide formed above interacts with protons or water on the surface of catalyst to produce hydroxyl radicals. It should be noted that no benzene oxidation occurs without peroxide as well as without UV irradiation, and both are required to be present together; in addition, molecular oxygen is required for high photocatalytic activity. The inert atmosphere created by bubbling Ar decreases the benzene conversion to a great extent, underscoring the role of molecular oxygen to produce hydroxyl radicals. Even though hydrogen peroxide was present in the experiment described above, the low benzene conversion demands the the *in situ* generation of hydroxyl radical for a larger amount of benzene conversion. The benzene radical ions react with hydroxyl

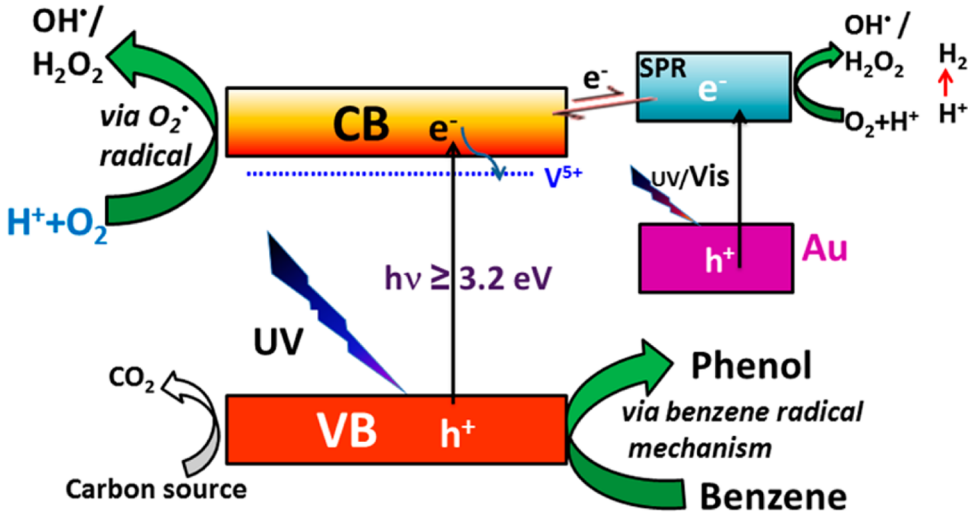

Figure 10. Possible mechanism of the photocatalytic oxidation of benzene to phenol, along with secondary reactions, proposed on the basis of experimental observations for Au/TV2. Primary reactions (benzene and O_2 conversion) occur on TV2 surfaces and are indicated by large green arrows; secondary reactions (CO_2 and H_2 formation) could occur on titania and gold surfaces. The energy gap shown for metallic gold indicates the surface plasmon resonance states. Schottky junction at the interface of Au and titania facilitates charge carrier separation upon light absorption. Because of the energy overlap between gold SPR states and the CB of TV2, electron transfer can occur between them, but predominantly from gold to TV2 (indicated by the larger arrow).

dx.doi.org/10.1021/cs500724z | ACS Catal. 2014, 4, 2844−2853

radical and form phenol, likely through the deprotonation of an unstable intermediate. Photocatalytic re-formation of acetonitrile, benzene, and/or phenol (mentioned as a carbon source in Figure 10) is the possible secondary reaction via the consumption of some holes on titania as well as gold, as there some amounts of CO_2 and H_2 were also observed in the gas phase products after irradiation.

Although nano gold can absorb visible light, much lower photocatalytic activity was observed on Au/TV2 in visible light. Enhancement of the emission features of Au/TV2 in PL reiterates the predominant transfer of the electron from gold to titania, leaving the holes in the VB of nano gold. However, because of the presence of Schottky junctions, the transfer of the electron from the CB of TV2 to Au can also trap the electrons for any reduction reactions on Au surfaces. It should be noted that the oxidation potential of holes in gold clusters is significantly lower than that of titania, suggesting the necessity of phenol formation in a highly facile manner exclusively on titania. A recent feature article reports the oxidation potential of benzene in an acetonitrile solvent to be 2.48 ± 0.03 eV.[36] This underscores the necessity of wide band gap semiconductors with a valence band maximum of ≥2.5 eV, which can be met only by titania in the system presented here. Above the benzene oxidation potential value is the possibility of oxidation exclusively on semiconductors, rather than metallic gold, which exhibits a significantly lower VB maximal energy (≤2 eV). Although visible light absorption does not help benzene oxidation for the reasons given above, it helps in reducing molecular oxygen to H_2O_2 as it occurs at a reduction potential of −0.695 eV. Parallel production of hydroxyl radicals on gold clusters and titania enhances benzene oxidation, and hence, a high level of conversion and a high phenol yield were observed on Au/TV2. Electrons in the CB of TiO_2 and plasmon excited state of gold could undergo three processes under the reaction conditions. (a) It may simply undergo recombination. (b) It could be consumed by H_2O_2 and/or by molecular oxygen to produce H_2O_2. (c) It could be trapped by V. Doubling of the phenol yield from 8% (TV2) to 16% (Au/TV2) underscores the prevalence of steps b and c, which aids the reaction. Nonetheless, we suggest time-resolved electron paramagnetic resonance studies of the reaction to improve our understanding and to precipitate further development of the catalyst.

4. CONCLUSION

We synthesized the UV active $Ti_{0.98}V_{0.02}O_2$ (TV2) semiconductor by a simple solution combustion synthesis protocol and Au/$Ti_{0.98}V_{0.02}O_2$ composites by photodeposition of gold on TV2. HRTEM and photoluminescence studies reveal the presence of Schottky junctions and an electron transfer mechanism between Au and titania, respectively. Charge carrier, especially hole, mobility is enhanced due to Schottky junctions on the disordered mesoporous structure along with electrically interconnected and electronically integrated nanocrystallites of Au and $Ti_{0.98}V_{0.02}O_2$. Moreover, the introduction of gold reduces the level of recombination of excited electron and hole and increases the separation and migration of electrons and holes to the surface of the catalyst for further reaction. The photocatalytic activity of Au/TV2 was studied by oxidation of benzene to phenol under UV irradiation. The introduction of vanadium and gold enhances the conversion of benzene and selectivity of phenol; 18% benzene conversion and 88.1 and 15.9% phenol selectivity and yield, respectively, in the presence of UV light, were obtained at ambient temperatures. Although nano gold absorbs visible light through SPR, Au/TV2 is not active for benzene oxidation under visible light because of the unavailability of holes on titania surfaces. Au and V act as electron sinks/traps, help in charge separation, and hence enhance the diffusion of holes on the titania surface and its utilization for oxidation. Nano gold does not seem to be catalytically active for benzene oxidation; rather, it helps to achieve a high phenol yield by charge carrier separation and increases the availability of holes on titania for oxidation.

■ ASSOCIATED CONTENT

Supporting Information

Spectral output from the UV source (Figure S1). This material is available free of charge via the Internet at http://pubs.acs.org.

■ AUTHOR INFORMATION

Corresponding Author

*Phone: +0091-20-2590 2043. Fax: +0091-20-2590 2633. E-mail: cs.gopinath@ncl.res.in.

Notes

The authors declare no competing financial interest.

■ ACKNOWLEDGMENTS

P.D. thanks UGC, New Delhi, for a research fellowship. We acknowledge the financial support from CSIR, New Delhi, to the TAPSUN program under Project NWP0056.

■ REFERENCES

(1) Fujishima, A.; Rao, T. N.; Tryk, D. A. *J. Photochem. Photobiol., C* **2000**, *1*, 1−21.
(2) Fujihira, M.; Satoh, Y.; Osa, T. *Nature* **1981**, *293*, 206−208.
(3) Palmisano, G.; Palmisano, L. *J. Adv. Synth. Catal.* **2007**, *349*, 964−970.
(4) (a) Ide, Y.; Matsuoka, M.; Ogawa, M. *J. Am. Chem. Soc.* **2010**, *132*, 16762−16764. (b) Ide, Y.; Nakamura, N.; Hattori, H.; Ogino, R.; Ogawa, M.; Sadakane, M.; Sano, T. *Chem. Commun.* **2011**, *47*, 11531−11533.
(5) (a) Zheng, Z.; Huang, B.; Qin, X.; Zhang, X.; Dai, Y.; Whangbo, M.-H. *J. Mater. Chem.* **2011**, *21*, 9079−9087. (b) Zheng, Z.; Huang, B.; Meng, X.; Wang, J.; Wang, S.; Lou, Z.; Wang, Z.; Qin, X.; Zhang, X.; Dai, Y. *Chem. Commun.* **2013**, *49*, 868−870.
(6) Tanarungsun, G.; Kiatkittipong, W.; Assabumrungrat, S.; Yamada, H.; Tagawa, T.; Praserthdam, P. *J. Chem. Eng. Jpn.* **2007**, *40*, 415−421.
(7) Chen, X.; Zhang, J.; Fu, X.; Antonietti, M.; Wang, X. *J. Am. Chem. Soc.* **2009**, *131*, 11658−11659.
(8) Zhang, P.; Gong, Y.; Li, H.; Chen, Z.; Wang, Y. *RSC Adv.* **2013**, *3*, 5121−5126.
(9) Bui, T. D.; Kimura, A.; Ikeda, S.; Matsumura, M. *J. Am. Chem. Soc.* **2010**, *132*, 8453−8458.
(10) (a) Herron, N.; Tolman, C. A. *J. Am. Chem. Soc.* **1987**, *109*, 2837−2839. (b) Mimoun, H.; Saussine, L.; Daire, E.; Postel, M.; Fischer, J.; Weiss, R. *J. Am. Chem. Soc.* **1983**, *105*, 3101−3110.
(11) Antonyraj, C. A.; Srinivasan, K. *Catal. Surv. Asia* **2013**, *17*, 47−70.
(12) (a) Sivaranjani, K.; Verma, A.; Gopinath, C. S. *Green Chem.* **2012**, *14*, 461−471. (b) Negi, S. S.; Sivaranjani, K.; Singh, A. P.; Gopinath, C. S. *Appl. Catal., A* **2013**, *452*, 132−138. (c) Shiju, N. R.; Anilkumar, M.; Mirajkar, S. P.; Gopinath, C. S.; Satyanarayana, C. V.; Rao, B. S. *J. Catal.* **2005**, *230*, 484−492.
(13) Cavani, F.; Cortelli, C.; Frattini, A.; Panzacchi, B.; Ravaglia, V.; Trifiro, F.; Fumagalli, C.; Leanza, R.; Mazzoni, G. *Catal. Today* **2006**, *118*, 298−306.
(14) Reddy, B. M.; Rao, K. N.; Reddy, G. K.; Bharali, P. *J. Mol. Catal. A: Chem.* **2006**, *253*, 44−51.
(15) Nielsen, U. G.; Topsoe, N. Y.; Brorson, M.; Skibsted, J.; Jakobsen, H. J. *J. Am. Chem. Soc.* **2004**, *126*, 4926−4933.

(16) Oganowski, W.; Hanuza, J.; Drulis, H.; Mista, W.; Macalik, L. *Appl. Catal., A* **1996**, *136*, 143−159.
(17) Kumar, C. P.; Reddy, K. R.; Rao, V. V.; Chary, K. V. R. *Green Chem.* **2002**, *4*, 513−516.
(18) Ye, X.; Yue, Y.; Miao, C.; Xie, Z.; Hua, W.; Gao, Z. *Green Chem.* **2005**, *7*, 524−528.
(19) Kim, S. S.; Pauly, T. R.; Pinnavaia, T. *Chem. Commun.* **2000**, 835−836.
(20) Zhang, Z.; Pinnavia, T. *J. Am. Chem. Soc.* **2002**, *124*, 12294−12301.
(21) (a) Sivaranjani, K.; Agarkar, S.; Ogale, S. B.; Gopinath, C. S. *J. Phys. Chem. C* **2012**, *116*, 2581−2587. (b) Gnanakumar, E. S.; John, J.; Raja, T.; Gopinath, C. S. *J. Nanosci. Nanotechnol.* **2013**, *13*, 2682−2688. (c) Mathew, T.; Sivaranjani, K.; Gnanakumar, E. S.; Yamada, Y.; Kobayashi, T.; Gopinath, C. S. *J. Mater. Chem.* **2012**, *22*, 13484−13493.
(22) (a) Mapa, M.; Gopinath, C. S. *Chem. Mater.* **2009**, *21*, 351−359. (b) Mapa, M.; Thushara, K. S.; Saha, B.; Chakraborty, P.; Janet, C. M.; Viswanath, R. P.; Nair, R. P.; Murty, K. V. G. K.; Gopinath, C. S. *Chem. Mater.* **2009**, *21*, 2973−2979. (c) Mapa, M.; Sivaranjani, K.; Bhange, D. S.; Saha, B.; Chakraborty, P.; Kasi Viswanath, A.; Gopinath, C. S. *Chem. Mater.* **2010**, *22*, 565−578.
(23) (a) Sivaranjani, K.; RajaAmbal, S.; Das, T.; Roy, K.; Bhattacharyya, S.; Gopinath, C. S. *ChemCatChem* **2014**, *6*, 522−530. (b) Sivaranjani, K.; Gopinath, C. S. *J. Mater. Chem.* **2011**, *21*, 2639−2647. (c) Naik, B.; Parida, K. M.; Gopinath, C. S. *J. Phys. Chem. C* **2010**, *114*, 19473−19482. (d) Satish, M.; Viswanathan, B.; Viswanath, R. P.; Gopinath, C. S. *Chem. Mater.* **2005**, *17*, 6349−6353. (e) Kulkarni, D. G.; Murugan, A. V.; Viswanath, A. K.; Gopinath, C. S. *J. Nanosci. Nanotechnol.* **2009**, *9*, 371−377. (f) Rajaambal, S.; Mapa, M.; Gopinath, C. S. *Dalton Trans.* **2014**, DOI: 10.1039/c4dt01268b.
(24) (a) Roy, K.; Vinod, C. P.; Gopinath, C. S. *J. Phys. Chem. C* **2013**, *117*, 4717−4726. (b) Roy, K.; Gopinath, C. S. *Anal. Chem.* **2014**, *86*, 3683−3687.
(25) (a) Maity, N.; Rajamohanan, P. R.; Ganapathy, S.; Gopinath, C. S.; Bhaduri, S.; Lahiri, G. K. *J. Phys. Chem. C* **2008**, *112*, 9428−9433. (b) Maity, P.; Gopinath, C. S.; Bhaduri, S.; Lahiri, G. K. *Green Chem.* **2009**, *11*, 554−561.
(26) Bulushev, D. A.; Kiwi Minsker, L.; Rainone, F.; Renken, A. *J. Catal.* **2002**, *205*, 115−122.
(27) Christodoulakis, A.; Machli, M.; Lemonidou, A. A.; Boghosian, S. *J. Catal.* **2004**, *222*, 293−306.
(28) Pantazidis, A.; Burrows, A.; Kiely, C. J.; Mirodatos, C. *J. Catal.* **1998**, *177*, 325−330.
(29) Yu, J. C.; Yu, J.; Ho, W.; Jiang, Z.; Zhang, L. *Chem. Mater.* **2002**, *14*, 3808−3816.
(30) Fujishima, A.; Zhang, X.; Tryk, D. A. *Surf. Sci. Rep.* **2008**, *63*, 515−582.
(31) (a) Bhattacharya, K.; Varma, S.; Tripathi, A. K.; Bharadwaj, S. R.; Tyagi, A. K. *J. Phys. Chem. C* **2008**, *112*, 19102−19112. (b) Zeferino, R. S.; Flores, M. B.; Pal, U. *J. Appl. Phys.* **2011**, *109*, 014308.
(32) (a) Das, N.; Eckert, H.; Hu, H.; Wachs, I. E.; Walzer, J. F.; Feher, F. J. *J. Phys. Chem.* **1993**, *97*, 8240−8243. (b) Rodella, C. B.; Franco, R. W. A.; Magon, C. J.; Donoso, J. P.; Nunes, L. A. O.; Saeki, M. J.; Aegerter, A.; Sargentelli, V.; Florentino, A. O. *J. Sol-Gel Sci. Technol.* **2003**, *25*, 83−88.
(33) (a) Satish, M.; Viswanath, R. P.; Gopinath, C. S. *J. Nanosci. Nanotechnol.* **2009**, *9*, 423−432. (b) Gopinath, C. S. *J. Phys. Chem. B* **2006**, *110*, 7079−7080.
(34) (a) Pandikumar, A.; Sivaranjani, K.; Gopinath, C. S.; Ramaraj, R. *RSC Adv.* **2013**, *3*, 13390−13398. (b) Sunil Sekhar, A. C.; Sivaranjani, K.; Gopinath, C. S.; Vinod, C. P. *Catal. Today* **2012**, *198*, 92−97.
(35) (a) Zhang, Y.; Zhang, N.; Tang, Z.-R.; Xu, Y.-J. *Chem. Sci.* **2012**, *3*, 2812−2822. (b) Sun, S.; Wang, W.; Zhang, L.; Zhou, L.; Yin, W.; Shang, M. *Environ. Sci. Technol.* **2009**, *43*, 2005−2010.
(36) Merkel, P. B.; Luo, P.; Dinnocenzo, J. P.; Farid, S. *J. Org. Chem.* **2009**, *74*, 5163−5173 and references cited therein.